J. Fluid Mech. (2022), *vol*. 951, A39, doi:10.1017/jfm.2022.881

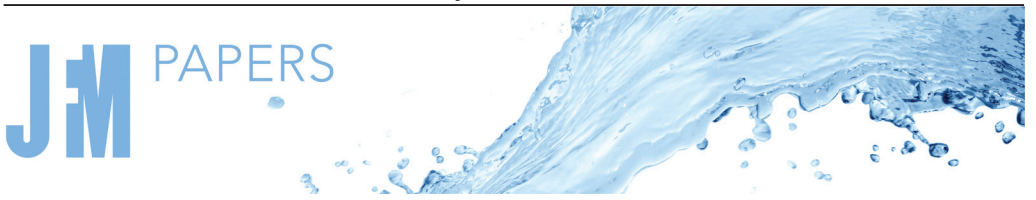

Physical mechanisms for droplet size and effective viscosity asymmetries in turbulent emulsions

Lei Yi[1], Cheng Wang[1], Thomas van Vuren[2], Detlef Lohse[3,4], Frédéric Risso[5], Federico Toschi[2,6] and Chao Sun[1,7,†]

[1]Center for Combustion Energy, Key Laboratory for Thermal Science and Power Engineering of Ministry of Education, Department of Energy and Power Engineering, Tsinghua University, 100084 Beijing, PR China

[2]Department of Physics and Department of Mathematics and Computer Science, Eindhoven University of Technology, 5600 MB Eindhoven, The Netherlands

[3]Physics of Fluids Group and Max Planck Center Twente, MESA+ Institute and J.M. Burgers Center for Fluid Dynamics, University of Twente, P.O. Box 217, 7500 AE Enschede, The Netherlands

[4]Max Planck Institute for Dynamics and Self-Organization, 37077 Göttingen, Germany

[5]Institut de Mécanique des Fluides de Toulouse (IMFT), Université de Toulouse, CNRS, Toulouse, France

[6]CNR-IAC, Via dei Taurini 19, 00185 Roma, Italy

[7]Department of Engineering Mechanics, School of Aerospace Engineering, Tsinghua University, Beijing 100084, PR China

(Received 19 January 2022; revised 18 July 2022; accepted 15 October 2022)

By varying the oil volume fraction, the microscopic droplet size and the macroscopic rheology of emulsions are investigated in a Taylor–Couette turbulent shear flow. Although here oil and water in the emulsions have almost the same physical properties (density and viscosity), unexpectedly, we find that oil-in-water (O/W) and water-in-oil (W/O) emulsions have very distinct hydrodynamic behaviours, i.e. the system is clearly asymmetric. By looking at the micro-scales, the average droplet diameter hardly changes with the oil volume fraction for O/W or for W/O. However, for W/O it is about 50 % larger than that of O/W. At the macro-scales, the effective viscosity of O/W is higher when compared to that of W/O. These asymmetric behaviours are expected to be caused by the presence of surface-active contaminants from the walls of the system. By introducing an oil-soluble surfactant at high concentration, remarkably, we recover the symmetry (droplet size and effective viscosity) between O/W and W/O emulsions. Based on this, we suggest a possible mechanism responsible for the initial asymmetry and reach conclusions on emulsions

† Email address for correspondence: chaosun@tsinghua.edu.cn

where interfaces are fully covered by the surfactant. Next, we discuss what sets the droplet size in turbulent emulsions. We uncover a $-6/5$ scaling dependence of the droplet size on the Reynolds number of the flow. Combining the scaling dependence and the droplet Weber number, we conclude that the droplet fragmentation, which determines the droplet size, occurs within the boundary layer and is controlled by the dynamic pressure caused by the gradient of the mean flow, as proposed by Levich (*Physicochemical Hydrodynamics*, Prentice-Hall, 1962), instead of the dynamic pressure due to turbulent fluctuations, as proposed by Kolmogorov (*Dokl. Akad. Nauk. SSSR*, vol. 66, 1949, pp. 825–828). The present findings provide an understanding of both the microscopic droplet formation and the macroscopic rheological behaviours in dynamic emulsification, and connects them.

Key words: multiphase flow, Taylor–Couette flow, turbulent convection

1. Introduction

Emulsions, such as mixtures of oil and water, have numerous industrial applications, including enhanced oil recovery, liquid–liquid extraction, drug delivery systems, and food processing (Mcclements 2007; Mandal *et al.* 2010; Maffi, Meira & Estenoz 2021). We can distinguish two types of emulsions: oil droplets in water and water droplets in oil, which we abbreviate with O/W and W/O, respectively (Salager *et al.* 2000). What emulsion type is realized depends on a number of variables, among which the dispersed phase volume fraction is determinant (Zambrano *et al.* 2003). Typically, by increasing the dispersed phase volume fraction ϕ_d, a point is reached where the system experiences a so-called catastrophic phase inversion, by which the dispersed phase suddenly becomes the continuous one, and vice versa (Piela, Ooms & Sengers 2009). The evolution from O/W to W/O (or vice versa) can be accompanied by a dramatic change of the emulsion properties, including its morphology, rheology and stability (Perazzo, Preziosi & Guido 2015). Various studies show that asymmetric behaviours between O/W and W/O emulsions can be found for both the phase inversion characteristics and hydrodynamic behaviours, such as the critical volume fraction for the phase inversion (Pacek, Nienow & Moore 1994), even when the densities and the viscosities of the two phases in an oil–water system are identical (Kumar 1996). In a gravity settler, W/O emulsions were found to separate much more rapidly than their O/W counterparts (Kato, Nakayama & Kawasaki 1991). The same holds for emulsions in a Taylor–Couette turbulent flow (Bakhuis *et al.* 2021). Additionally, it is found that O/W and W/O emulsions have different structures for a volume fraction $\phi_d > 25\,\%$ of the dispersed phase (Pacek *et al.* 1994). These experimental findings of the asymmetry in emulsions cannot be explained easily within the scope of existing models (Kumar 1996). Although some models (e.g. charged droplet model) have been proposed to account for the above-mentioned observations (Kumar 1996; Tobin & Ramkrishna 1999), the understanding of asymmetric behaviours between O/W and W/O emulsions is still very limited.

Turbulent emulsions are complex physical systems, characterized by a dynamical coupling between small-scale droplets, large-scale flow and rheology. In the low-volume-fraction regime, droplet fragmentation is generally caused by the turbulent stress, while the presence of droplets hardly affects the continuous phase (Afshar Ghotli *et al.* 2013). The study of the droplet size in a turbulent flow can be traced back to Kolmogorov (1949) and Hinze (1955), who attributed the droplet breakup to

turbulent fluctuations. Although the Kolmogorov–Hinze (K–H) theory has been validated in a variety of experimental and numerical studies on droplets or bubbles in a turbulent flow (Risso & Fabre 1998; Perlekar *et al.* 2012; Eskin, Taylor & Yang 2017; Rosti *et al.* 2019), it was found to have limitations, for example, in non-homogeneous turbulent flows (Hinze 1955). In the high-volume-fraction regime (before phase inversion), the microscopic droplet structure (droplet size and distribution) generated by the turbulent stresses has a strong feedback on the macroscopic properties (viscosity) of the turbulent emulsion (De Vita *et al.* 2019; Yi, Toschi & Sun 2021). It has been found that the effective viscosity of the emulsion increases with increasing the volume fraction of the dispersed phase, which is similar to what is found for the case of suspensions of solid particles (Stickel & Powell 2005; Guazzelli & Pouliquen 2018; Rosti & Takagi 2021). However, when considering the statistics of deformation, coalescence and breakup, the dynamics of the droplets in emulsions is expected to be much richer than that of solid particles in suspensions.

The problem becomes even more complicated when we consider turbulent emulsions in practical environmental and industrial applications, where the appearance of dirt and surfactant in liquids or on the interfaces has to be taken into account (Bazazi & Hejazi 2020; Soligo, Roccon & Soldati 2020). The surfactant dynamics can strongly modify the evolution of a flowing emulsion. On the one hand, the surfactant directly changes the interfacial properties, affecting the interface deformation and collision rate (Manikantan & Squires 2020). On the other hand, the presence of surfactant can alter the global properties of the emulsion, such as its rheology (Kawaguchi 2016). However, the current understanding of the physics of turbulent emulsions with surfactant addition is still limited.

In this work, we study the dynamics of the emulsion in a turbulent shear flow, with an oil volume fraction ranging from 0 % to 100 %. We focus on the dispersed droplet size as a microscopic observer, and the effective viscosity of the emulsion as a macroscopic observer. By introducing a surfactant at a controlled concentration into the system, we aim to reveal the physical mechanism for the asymmetric behaviours between O/W and W/O emulsions. Furthermore, we uncover the breakup mechanism of the droplet in such turbulent emulsions, for which the droplet Weber number plays a crucial role.

2. Experimental set-up and procedure

In this study, the emulsion consists of two immiscible liquids: silicone oil (density $\rho_o = 866$ kg m^{-3} and viscosity $\nu_o = 2.1 \times 10^{-6}$ m^2 s^{-1}) and an aqueous mixture of ultra-pure water and ethanol ($\rho_w = 860$ kg m^{-3}, $\nu_w = 2.4 \times 10^{-6}$ m^2 s^{-1}). The experiments were carried out in a Taylor–Couette (TC) system (see figure 1). The system has inner cylinder radius $r_i = 25$ mm, outer cylinder radius $r_o = 35$ mm, and gap $d = 10$ mm, giving a radius ratio $\eta = r_i/r_o = 0.71$. The height of the inner cylinder is $L = 75$ mm, so that the aspect ratio is $\Gamma = L/d = 7.5$. The inner cylinder is made of aluminium, while the outer one is made of glass to enable optical measurements. Initially, the gap between the cylinders is filled by the ethanol–water mixture and the oil. Then the inner cylinder is set in rotation at a constant angular velocity ω_i, while the outer cylinder is kept fixed (i.e. $\omega_o = 0$). A strong turbulent shear flow is generated, producing an emulsion. After a certain time, the emulsion finally reaches a state where its statistical properties are steady. Note that the density match of the two phases (oil and ethanol–water) eliminates the effect of the centrifugal force on the liquid distribution in the system (see Appendix A). A circulating water bath is used to maintain the working temperature at $\theta = 22 \pm 0.1\,^{\circ}$C. The temperature gradient in the emulsion is negligible due to the efficient mixing induced

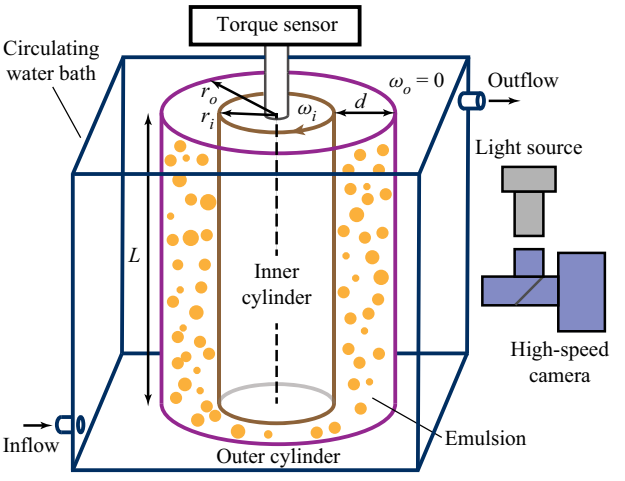

Figure 1. Sketch of the experimental set-up. The gap between the inner and outer cylinders is filled with two immiscible liquids: silicone oil and ethanol–water. The emulsion is formed by rotating the inner cylinder at a given angular velocity ω_i, while the outer cylinder is kept fixed. The torque of the inner cylinder is measured by a torque sensor. A circulating water bath is used to maintain the working temperature at $\theta = 22 \pm 0.1\,^{\circ}\mathrm{C}$. A high-speed camera equipped with a long-distance microscope is used to capture the dispersed droplets in the flow.

by the turbulent fluctuations (van Gils *et al.* 2011; Grossmann, Lohse & Sun 2016). The control parameter of the TC flow is the Reynolds number defined as $Re = \omega_i r_i d/\nu_w$, where ω_i is the imposed angular velocity of the inner cylinder, and ν_w is the viscosity of the ethanol–water. Here, we also define a modified Reynolds number $Re_m = \omega_i r_i d/\nu_{eff}$, where ν_{eff} is the effective viscosity of the emulsion. We measured the total torque exerted on the inner cylinder T_{raw}, which includes two parts: the torque contribution T from the cylindrical sidewall surfaces (the TC flow), and the torque contribution T_{end} from both the top and bottom end plates (the end flow). Here, T_{end} is measured using the same linearization method as in previous studies (Hu *et al.* 2017; Greidanus, Delfos & Westerweel 2011) (see Appendix B). Thus the torque contribution of the TC flow can be determined by $T = T_{raw} - T_{end}$. Based on this, the dynamic response of the emulsion to the imposed rotation is characterized by the dimensionless torque $G = T/2\pi L\rho\nu_w^2$, and a modified one, $G_m = T/2\pi L\rho\nu_{eff}^2$.

The dispersed oil (or ethanol–water) droplets in the emulsion were captured using the high-speed camera equipped with a long-distance microscope. Videos and images from experiments were analysed for the drop size determination using ImageJ software and Matlab codes. The numerical average of the droplet diameter, $\langle D\rangle$, is used as the indicator of the droplet size in this study. To ensure that we achieve enough statistics, the average droplet diameter is calculated based on $O(10^3)$ droplet samples. Experiments were performed for various oil volume fractions ϕ_o and Reynolds numbers Re.

3. Results and discussion

3.1. *Asymmetric behaviours of the droplet size and the effective viscosity*

The size of the dispersed droplets in a turbulent emulsion characterizes the microscopic structure of the emulsion, which affects the macroscopic stability and rheology of

the emulsion. Also, the volume fraction of the dispersed phase, ϕ_d, determines both the micro-scale structure (droplet size) and, consequently, the macro-scale rheological behaviours (effective viscosity).

First, we focus on the effect of the oil volume fraction, ϕ_o, on the droplet size, for a given Reynolds number $Re = 5.2 \times 10^3$. The volume fraction of oil, ϕ_o, is varied from 0 (ethanol–water mixture) to 100 % (pure oil) by fixing the volume of each phase initially put into the TC system. After emulsification, the final state of the emulsion is observed to be O/W for $\phi_o \leqslant 50\,\%$, and W/O for $\phi_o \geqslant 60\,\%$. A phase inversion, in which the continuous phase and the dispersed phase are exchanged (Salager *et al.* 2000; Bakhuis *et al.* 2021), is thus expected to occur in between these two volume fractions. Note that the transient process of phase inversion, which consists of distinct runs at various volume fractions, is not observed in the present experiments. In this range, the behaviour of the system is too complex to allow for an accurate determination of the inversion point. In the following, we will consider only values of ϕ_o either below 50 % or larger than 60 %, for which the natures of the dispersed and continuous phases are determined unambiguously. In this study, we focus on the global and local properties of O/W and W/O emulsions in a turbulent flow. Note that all emulsions that we obtained are of a simple type, and we did not observe multiple emulsions, such as O/W/O or W/O/W (Perazzo *et al.* 2015). A typical O/W emulsion for $\phi_o = 5\,\%$ and W/O emulsion for $\phi_o = 95\,\%$ are shown in inset images in figure 2(*a*). Under steady stirring conditions, the droplet size in the turbulent emulsion eventually shows a statistically stationary distribution, giving an average of the droplet diameter $\langle D \rangle$ as an indicator for the droplet size. The average droplet diameters for various oil fractions are shown in figure 2(*a*). For both O/W emulsions (left branch, $\phi_o \leqslant 50\,\%$) and W/O emulsions (right branch, $\phi_o \geqslant 60\,\%$), it is found that the droplet size is almost independent of the oil fraction, at fixed Re. Remarkably, we find that the ethanol–water droplets in the right branch are about 50 % larger than the oil droplets in the left branch, indicating an obvious asymmetry of the droplet size between O/W and W/O emulsions. One may think that this asymmetric behaviour is due to the slight difference in physical properties of the two liquids used in experiments. However, we note that the densities of these two liquids are too close to account for the observed asymmetry. The interfacial tension between the two immiscible liquids is also identical for O/W and W/O emulsions. What about the viscosity? The viscosity of the silicone oil, $\nu_o = 2.1 \times 10^{-6}$ m^2 s^{-1}, is slightly lower than that of the ethanol–water, $\nu_w = 2.4 \times 10^{-6}$m^2 s^{-1}, at the experimental temperature $\theta = 22\,^{\circ}$C, while it has been found that at least an order of magnitude difference between the viscosities of the two phases could change the droplet size by a measurable amount (Pacek *et al.* 1994). Moreover, additional experiments that we have performed show that the asymmetry of the droplet size remains even when we eliminate viscosity difference by adjusting the working temperature (see Appendix D for more details). Thus the small viscosity difference cannot account for the observed asymmetry of the droplet size in these experiments. The asymmetry of the droplet size must therefore have another origin.

Apart from the droplet size, also the effective viscosity of the emulsion shows an asymmetric behaviour. For various oil volume fractions ($0\,\% \leqslant \phi_o \leqslant 100\,\%$), we measured the effective viscosity of the emulsion, ν_{eff}, which is calculated using a method that has been proposed recently for viscosity measurements in a turbulent TC flow (Bakhuis *et al.* 2021; Yi *et al.* 2021). As is well known, an effective power-law dependence $G \propto Re^{\alpha}$ holds in the single-phase TC turbulent flow, where the power-law

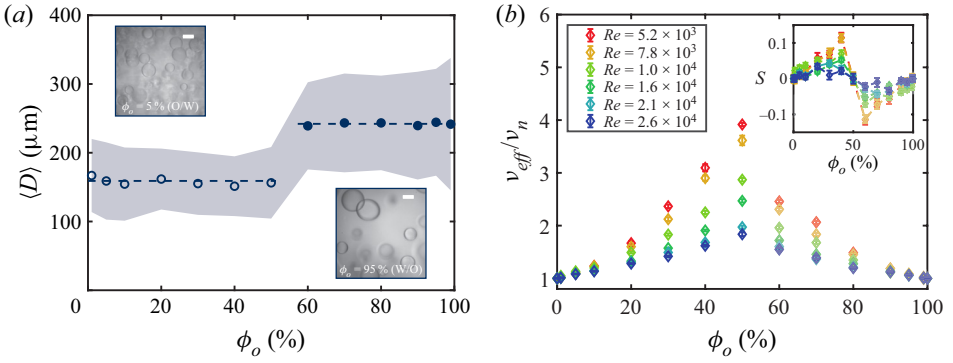

Figure 2. (*a*) Average droplet diameter as a function of the oil volume fraction. The droplet diameter hardly changes with the oil volume fraction for both O/W emulsions ($\phi_o \leqslant 50\,\%$, hollow points) and W/O emulsions ($\phi_o \geqslant 60\,\%$, solid points). The ethanol–water droplets in W/O are found to be about 50 % larger than the oil droplets in O/W. The bluish band spans one standard deviation around the average diameter. The dashed lines denote the average values of the droplet diameters for O/W (or W/O). A typical O/W emulsion ($\phi_o = 5\,\%$) and a typical W/O emulsion ($\phi_o = 95\,\%$) are shown in the insets. The scale bar represents 200 μm. (*b*) The normalized effective viscosity of the emulsion as a function of the oil volume fraction ϕ_o for various Reynolds numbers Re. The inset shows the asymmetry factor S as a function of ϕ_o for various ω_i. The asymmetric trend of the effective viscosity between O/W (left branch) and W/O (right branch) emulsions is more pronounced at low Reynolds numbers.

exponent α depends on the regime of the Reynolds number (Grossmann *et al.* 2016). Indeed, if the modified Reynolds number and dimensionless torque are used, then the current two-phase emulsion flow still follows the effective power-law dependence $G_m \propto Re_m^{\alpha}$, where $\alpha = 1.58$ in this study (see Appendix B). Based on this relation, we can calculate the effective viscosity of the emulsion, ν_{eff}. The detailed calculation of the effective viscosity is documented in Appendix B. The results of the effective viscosity are shown in figure 2(*b*), which can also be divided into two parts: O/W emulsions for $\phi_o \leqslant 50\,\%$ (left branch), and W/O emulsions for $\phi_o \geqslant 60\,\%$ (right branch). Here, the effective viscosity is characterized by its normalized value, ν_{eff}/ν_n, where $\nu_n = \nu_w$ for O/W ($\phi_o \leqslant 50\,\%$), and $\nu_n = \nu_o$ for W/O ($\phi_o \geqslant 60\,\%$). For each branch, the effective viscosity increases with the increasing dispersed phase volume fraction ϕ_d for all Reynolds numbers. Note that the dispersed phase refers to oil for O/W or ethanol–water for W/O. The effective viscosity has only a weak dependence on the dispersed phase volume fraction in the dilute regime (i.e. for $\phi_d < 5\,\%$), while it displays a stronger dependence at larger dispersed phase volume fractions. The increase of the effective viscosity with increasing ϕ_d originates from the hydrodynamic or contact interactions between dispersed droplets, as it is observed in similar turbulent droplet dispersions (Pouplin *et al.* 2011) and in solid particle suspensions (Guazzelli & Pouliquen 2018). Furthermore, the effective viscosity is found to decrease with the increasing Reynolds number for a given ϕ_d, indicating that the turbulent emulsion somehow shows a shear-thinning behaviour (Yi *et al.* 2021). Though the qualitative trend of the effective viscosity versus the dispersed phase volume fraction is similar for both the left and right branches, an asymmetry of the effective viscosity between O/W and W/O emulsions is measured. The effective viscosity of O/W (left branch) is found to be higher than that of W/O (right branch) for a given Reynolds number, particularly for the case of the high dispersed phase volume fraction (see figure 2*b*). To represent quantitatively the degree of asymmetry, we define an asymmetry

factor as

$$S = \frac{\left(\frac{\nu_{eff}}{\nu_n}\right)_{\phi_o} - \left(\frac{\nu_{eff}}{\nu_n}\right)_{1-\phi_o}}{\left(\frac{\nu_{eff}}{\nu_n}\right)_{\phi_o} + \left(\frac{\nu_{eff}}{\nu_n}\right)_{1-\phi_o}}, \tag{3.1}$$

where the subscripts ϕ_o and $1-\phi_o$ denote the emulsion at ϕ_o and at $1-\phi_o$, respectively. An asymmetry factor S deviating from 0 indicates asymmetry. The asymmetry factor, as a function of the oil volume fraction, is shown as the inset of figure 2(*b*). It is found that the asymmetry decreases with the increasing Reynolds number. In addition, the asymmetric trend between O/W and W/O is more pronounced for high dispersed phase volume fractions. Since it was already found that the droplet size has a dramatic influence on the emulsion rheology (Pal 1996), the macroscopic asymmetry of the effective viscosity between O/W and W/O could be connected to the microscopic asymmetric behaviour of the droplet size.

3.2. *Recovering the asymmetry between O/W and W/O emulsions using surfactant*

We hypothesize that the possible reason for the asymmetry of the droplet size between O/W and W/O emulsions is the presence of surface-active contaminants. These surface-active contaminants are found widely on the liquid–liquid interface in practical environments, which is focused on by various studies related to interfacial phenomena (de Gennes 2001; De Malmazet *et al.* 2015; Calvo *et al.* 2019). On the one hand, these surface-active contaminants can modify the interfacial properties, yielding the change of the droplet size in the emulsion (Bazazi & Hejazi 2020; Manikantan & Squires 2020). On the other hand, the solubility of these contaminants is usually different in the oil phase and the aqueous phase (Kawaguchi 2016). The preferential solubility can induce a different distribution of contaminants and different interfacial properties in O/W and W/O, which could be the source of the asymmetric behaviours.

To investigate the effect of surfactants on the asymmetric behaviour of turbulent emulsions, an effective way is to add a controlled amount of a selected surfactant into the system. First, we perform experiments using a kind of oil-soluble non-ionic surfactant: dimethylsiloxane block copolymer (30–35 % ethylene oxide). For convenience, we use its abbreviation (DBE) from the manufacturer. For the purpose of the present study, two contrasted concentrations of DBE in oil are selected. One is 12.5 μl l^{-1}, which is comparable to the critical micelle concentration (CMC) of DBE in water (around 13 μl l^{-1}) (Rheingans *et al.* 2000), and the second, 20 times larger, is 250 μl l^{-1}. The DBE is well mixed with the oil before each experiment. Two microscopic images of O/W and W/O emulsions with added 250 μl l^{-1} DBE are shown in figure 3(*b*). Figure 3(*c*) shows the results of the droplet size in emulsions using DBE, for various oil volume fractions. Here, the Reynolds number is fixed at $Re = 5.2 \times 10^3$. The measured droplet sizes for emulsions using 12.5 μl l^{-1} and 250 μl l^{-1} DBE are denoted by yellow marks and red marks in figure 3(*c*), respectively. It is found that DBE only slightly reduces the droplet size in O/W emulsions (left branch) when compared to what has been found in emulsions without adding surfactant (blue marks). But for W/O emulsions (right branch), the droplet size decreases with the increasing concentration of DBE. When 250 μl l^{-1} DBE is used, remarkably, the droplet size difference between O/W and W/O emulsions is eliminated (see red marks in figure 3*c*). Consequently, we nearly recover the symmetry of the droplet

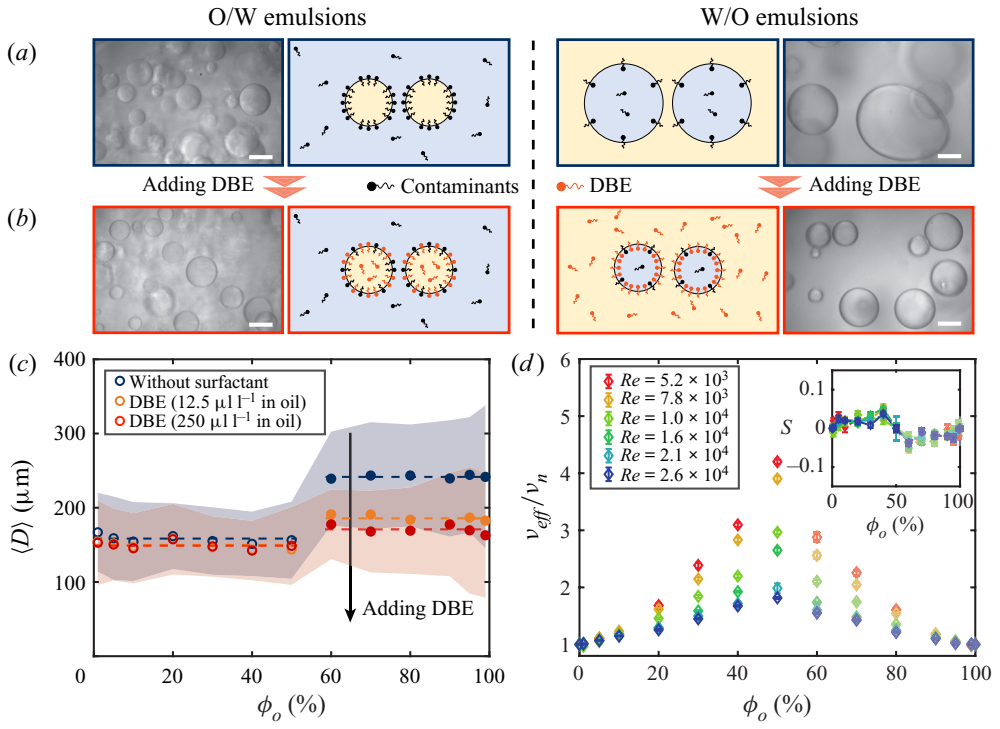

Figure 3. (*a*,*b*) Schematic diagrams and microscopic images of the effects of surfactants (or surface-active contaminants) on the emulsions. Panel (*a*) depicts the emulsions without adding surfactant. The asymmetric behaviours of the droplet size between O/W emulsions and W/O emulsions are observed due to the difference in the concentrations of contaminants on the interfaces. The deformation of the droplet is observed clearly in W/O emulsions. Panel (*b*) represents emulsions with added DBE at 250 $\mu l\,l^{-1}$. The surfactant is adsorbed into the interface at saturation for both O/W and W/O emulsions. The symmetry of droplet size is almost recovered. Snapshots of the emulsion at an oil volume fraction $\phi_o = 5\,\%$ are used to represent O/W emulsions, while W/O emulsions are denoted by snapshots of the emulsion at $\phi_o = 95\,\%$. For all snapshots here, $Re = 5.2 \times 10^3$. The scale bar represents 200 μm. (*c*) The droplets size in emulsions for various oil volume fractions, with and without adding the surfactant, for $Re = 5.2 \times 10^3$. The droplet size almost does not change with the oil volume fraction for both O/W ($\phi_o \leqslant 50\,\%$) and W/O ($\phi_o \geqslant 60\,\%$) emulsions. The asymmetric trends of the droplet size between O/W and W/O are found to disappear when adding surfactant DBE into the emulsion systems. Note that 12.5 $\mu l\,l^{-1}$ and 250 $\mu l\,l^{-1}$ here refer to the concentrations of DBE in oil. The dashed lines represent the average values of the droplet diameters for O/W (or W/O). The coloured bands span the average diameter ± one standard deviation. For the sake of clarity, the coloured band for the case using 12.5 $\mu l\,l^{-1}$ DBE is not present here. (*d*) The normalized effective viscosity of the emulsion for the oil volume fraction from $\phi_o = 0\,\%$ to $\phi_o = 100\,\%$, with added surfactant DBE at 250 $\mu l\,l^{-1}$, at various Reynolds numbers. The inset shows the asymmetry factor S as a function of the oil volume fraction. The asymmetric behaviour of the effective viscosity between O/W and W/O emulsions becomes considerably smaller due to the presence of surfactant DBE at saturation.

size between O/W and W/O by adding oil-soluble surfactant DBE at high concentration into the emulsion system.

The above results can be explained using the schematic diagrams in figures 3(*a*,*b*). We first focus on the cases without adding surfactant. In the practical environment, even in careful laboratory experiments, the emulsion inevitably contains some surface-active contaminants (Duineveld 1995; Lalanne, Masbernat & Risso 2020; Soligo *et al.* 2020) (black indicators in figure 3*a*), which could originate from the wall of the container in

Re	5.2×10^3	7.8×10^3	1.0×10^4	1.6×10^4	2.1×10^4	2.6×10^4
$\langle D \rangle / \lambda_u$	0.2	0.2	0.2	0.1	0.1	0.1
$\langle D \rangle / \delta_{vis}$	0.8	0.7	0.6	0.6	0.5	0.5
$\langle D \rangle / \eta_{bl}$	2.1	1.7	1.6	1.4	1.2	1.1
Ca	0.02	0.03	0.03	0.04	0.04	0.04

Table 1. Some comparisons of length scales and capillary number. The O/W case at $\phi_o = 1\,\%$ is used here. Detailed calculations can be found in Appendix C.

this study. These surface-active contaminants are expected to be preferentially soluble in the aqueous ethanol–water, a quite good solvent, and act as a surfactant. As illustrated in the left-hand part of figure 3(*a*) (O/W), the surface-active contaminants from the wall dissolve into the continuous phase of ethanol–water. These contaminants are then adsorbed onto the liquid–liquid interface and modify the oil droplet size for two reasons. On the one hand, contaminants on the surface suppress droplet coalescence, which is known to be a common effect of surfactants on emulsion systems (Cristini, Bławzdziewicz & Loewenberg 1998; Ha, Yoon & Leal 2003; Dai & Leal 2008; Baret 2012). On the other hand, these surface-active contaminants cover the surface of oil droplets, inducing a reduction of the interfacial tension (Manikantan & Squires 2020). Thus the breakup of droplets could be promoted. The effect of contaminants on the breakup and coalescence of the droplets finally reflects on the smaller size of oil droplets in O/W. As the interfacial tension is found to decrease only slightly with the concentration of DBE (see Appendix A), it is reasonable to assume that the inhibition of the droplet coalescence is the dominant factor affecting the droplet size here. However, when oil is the continuous phase (W/O), as shown in the right-hand part of figure 3(*a*), ethanol–water droplets embedded within the oil are not in contact with walls. Therefore, only a limited amount of surface-active contaminants are adsorbed onto the interface. The cleaner liquid–liquid interface brings less inhibition to the coalescence, yielding the larger droplet size for the given turbulent strength (see figure 3*a*). It should be noted that the difference between the O/W and W/O cases is not that there are surfactants in one case and no surfactant in the other case. The different behaviours arise from the fact that in the O/W case, the interfaces are fully covered by surfactants, which inhibit coalescence, and in the W/O case, there is not enough surfactant to significantly cover interfaces and inhibit coalescence.

The effective viscosity difference between O/W and W/O could be related to the deformability of the dispersed phase, which is closely connected to the droplet size (Verschoof *et al.* 2016; Bakhuis *et al.* 2021). When compared to the larger ethanol–water droplets, the small and non-deformable oil droplets could behave as solid-like particles and bring an extra contribution to the effective viscosity of the emulsion in a turbulent flow (Bakhuis *et al.* 2018; Guazzelli & Pouliquen 2018). In addition, as the droplet size is found to be comparable with the viscous sublayer thickness δ_{vis} (see table 1 below, and Appendix C), the exclusion of the droplets from the viscous sublayer could also be a reason for the reduced effectiveness of larger drops on the effective viscosity in W/O emulsions. Furthermore, surface-active contaminants in W/O could modify the dynamics of the emulsion through the hydrodynamic coupling interaction between the oil-droplet surface and the surrounding flow (Baret 2012). As a result, the surface-active contaminants account for the measured higher effective viscosity of O/W (left branch) compared to that of W/O (right branch) (see figure 3*b*).

Next, we consider the experimental results using the oil-soluble surfactant DBE. For the case of O/W emulsion shown in the left-hand part of figure 3(*b*), some DBE added in the system is competitively adsorbed into the interface. As the interface is already saturated due to the contaminants, the interfacial properties show no significant change when adding DBE, which is consistent with the previous result that the droplet sizes for O/W emulsions decrease only slightly when DBE is added. When the oil is the continuous phase (W/O) as shown in the right-hand part of figure 3(*b*), the surface of ethanol–water droplets is expected to be mostly covered by DBE adsorbed from oil, i.e. the surface is at saturation ($250\ \mu l\,l^{-1}$ case). Therefore, the coalescence of droplets is now inhibited. Consequently, the asymmetric trend of the droplet size between O/W and W/O is eliminated using DBE (figure 3*c*).

In this part, we focus on the effect of surfactant on another feature of the emulsion system: the effective viscosity. As shown in figure 3(*d*), it is found that the symmetry of the effective viscosity between O/W (left branch) and W/O (right branch) emulsions is partially recovered using $250\ \mu l\,l^{-1}$ DBE. This is clearly indicated by the asymmetry factor S close to 0 (see the inset of figure 3*d*), which is expected to be mainly attributed to the recovery of the symmetry of the droplet size using DBE (see figure 3*c*). It should be noted that the symmetry of the effective viscosity is not fully recovered. In general, there are always some differences between O/W and W/O emulsions, such as the distribution of the surfactant in the flow. The effective viscosity for each case is found to be slightly larger than that for its corresponding case without adding surfactant (compare figures 3(*d*) and 3(*b*)). The reason could be that the polymeric surfactant (DBE in this study) with high molecular weight enhances the interfacial rigidification effect of the droplet surface when compared to the case with only contaminants (Erni 2011). Indeed, the copolymer molecules of surfactant could form shell-like structures around the drops (Sundararaj & Macosko 1995). This increases the resistance of the droplet to the surrounding flow, yielding the extra contribution of the viscous dissipation of the flow. Note that although there is still some uncertainty about the presence of the contaminant due to limitation of the experiments, the recovery of the symmetry using oil-soluble surfactant DBE supports the hypothesis that surface-active contaminants are the cause of the asymmetry.

3.3. *The dependence of the droplet size on the Reynolds number*

As the droplet size and the associated asymmetry have been discussed for various oil fractions, the next question is what sets the droplet size in turbulent emulsions. In this part, we study the dependence of the droplet size on the Reynolds number, at the low volume fraction of the dispersed phase (i.e. $\phi_o = 1\,\%$ and $99\,\%$). Since the volume fraction of the dispersed phase is very low in these cases, the viscosity of the emulsion is approximately equal to that of the continuous phase, giving $Re_m \approx Re$ and $G_m \approx G$. We first consider the cases at $\phi_o = 1\,\%$ without using surfactant. Note that the coalescence of droplets is inhibited due to the surface-active contaminants on the droplet surface. Therefore, the droplet size is determined mainly by the turbulent breakup mechanism. As shown in figure 4(*a*) by the black circles, the droplet size normalized by the gap, $\langle D\rangle/d$, is found to have a scaling dependence on the Reynolds number Re with effective exponent -1.18 ± 0.05 obtained by a direct fit for $\phi_o = 1\,\%$.

We now explore the physical mechanism behind the scaling dependence of the droplet size on the Reynolds number. According to the K–H theory, the droplet formation in a turbulent flow is determined by the competition between the deforming external dynamic pressure force (turbulent fluctuations) and the resisting interfacial tension over the droplet

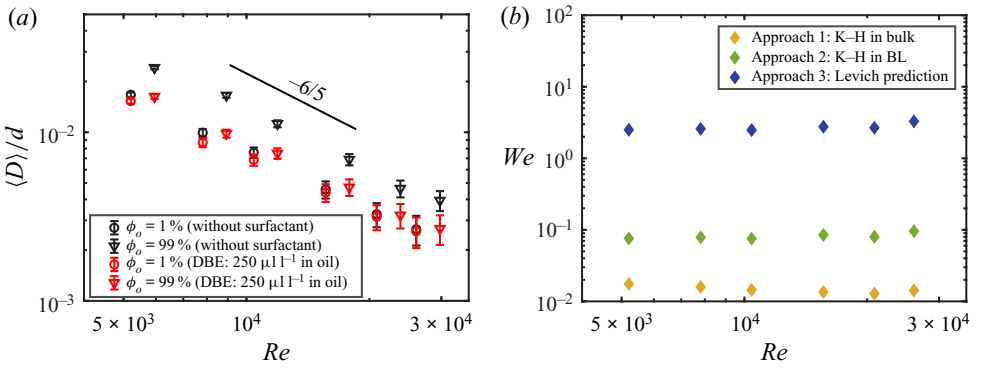

Figure 4. (*a*) The average droplet diameter normalized by the gap width as a function of the Reynolds number for oil volume fractions $\phi_o = 1\,\%$ and $99\,\%$. The black and red symbols denote droplet sizes in emulsions using no surfactant and using 250 μl l^{-1} DBE, respectively. The error bars are based on the errors of the edge detection. The black lines denote the scaling prediction of the Kolmogorov–Hinze (K–H) theory, $\langle D\rangle/d \sim Re^{-6/5}$. The asymmetry of the droplet size in O/W ($\phi_o = 1\,\%$) and W/O ($\phi_o = 99\,\%$) emulsions is removed using DBE at saturation. (*b*) The Weber number as a function of the Reynolds number in a log-log plot for the two theoretical approaches. The yellow, green and blue diamonds denote the results using K–H theory based on the energy dissipation rate in the bulk area, that using K–H theory based on energy dissipation rate in the boundary layer (BL), and that using Levich's theory, respectively. The O/W emulsions at $\phi_o = 1\,\%$ without surfactant are considered here.

surface (Kolmogorov 1949; Hinze 1955), of which the ratio is usually indicated by the droplet turbulent Weber number $We = \rho\,\overline{\delta u^2}\,D/\gamma$, where ρ is the density of the continuous phase, $\overline{\delta u^2}$ is the mean-square velocity difference over a distance equal to the droplet diameter D, and γ is the interfacial tension between the two phases (Risso & Fabre 1998). If the droplet diameter D belongs to the inertial turbulent sub-range, then $\overline{\delta u^2}$ could be expressed as a function of the local energy dissipation rate: $\overline{\delta u^2} = C_1(\varepsilon D)^{2/3}$, where the constant is $C_1 \approx 2$ according to Batchelor (1953). This yields the Weber number as $We = 2\rho\varepsilon^{2/3}D^{5/3}/\gamma$. The force balance implies the existence of a critical value of the Weber number beyond which breakup occurs (Hinze 1955), and this value is found to be of the order of unity (i.e. $We \sim O(1)$) in various studies (Hesketh, Etchells & Russell 1991*a*; Risso & Fabre 1998; Lemenand *et al.* 2017). Thus the prediction of the maximum stable droplet size in a homogeneous and isotropic turbulent flow can be given by $D_{max} = C(\rho/\gamma)^{-3/5}\varepsilon^{-2/5}$ (where C is a constant coefficient), which is the main result of the work by Hinze (1955). Moreover, various studies have shown that the average droplet diameter $\langle D\rangle$ can be used as the indicator of the droplet size in the K–H prediction (Lemenand *et al.* 2003; Boxall *et al.* 2012; Perlekar *et al.* 2012).

First, we speculate that the droplet size could be dominated by the turbulent fluctuations in the bulk flow of the system, where most droplets distribute. The local energy dissipation rate in the bulk can be estimated as $\varepsilon_b \sim u_T^3/\ell$, where u_T and ℓ are the typical velocity fluctuation and the characteristic length scale of the flow (Ezeta *et al.* 2018). As the typical velocity fluctuation can be expressed as $u_T \sim \omega_i r_i \sim Re\,\nu/d$ (Van Gils *et al.* 2012), we obtain $\varepsilon_b \sim Re^3\nu^3/d^4$ by assuming $\ell \sim d$. Inserting ε_b into the K–H prediction, the scaling dependence of the droplet size on the Reynolds number is obtained as $\langle D\rangle/d \sim Re^{-6/5}$, which agrees well with the experimental results for $\phi_o = 1\,\%$ without surfactant (see black circles in figure 4*a*). However, the discussion above is only a simple analysis based on

the scaling law. A further quantitative study on the droplet formation in a turbulent flow needs to consider the Weber number, which can be calculated as $We = 2\rho_w \varepsilon_b^{2/3} D^{5/3}/\gamma$, where ε_b can be estimated as $\varepsilon_b \approx 0.1 T\omega_i/[\pi(r_o^2 - r_i^2)L\rho_w]$ in a TC turbulent flow (Ezeta *et al.* 2018). As shown in figure 4(*b*) (yellow diamonds, approach 1), the Weber number ranges between 0.013 and 0.018, two orders of magnitude smaller than the critical value obtained in previous studies, suggesting that the bulk of the system, where most droplets flow around, is not the place where the droplet size is determined.

Indeed, the droplet breakup is most often observed close to the area where the most intense stress participates in the deformation (Hesketh, Etchells & Russell 1991*b*; Afshar Ghotli *et al.* 2013). Considering that the coalescence is almost inhibited in the current system, the droplet size is dominated mainly by the place where small droplets are generated. Thus the droplet size is expected to be dominated by the boundary layer area close to the wall, where the K–H theory has some limitations. First, as shown in table 1, the droplet size is found to be smaller than the turbulent boundary layer thickness ($\langle D\rangle/\lambda_u < 1$), which supports the occurrence of breakup in the boundary layer. The droplet size is larger than the Kolmogorov length scale in the turbulent boundary layer ($\langle D\rangle/\eta_{bl} > 1$). Additionally, the results for the capillary number are of the order of 10^{-2}, indicating the negligible effect of the viscous deforming stress on the determination of the droplet size. Next, we check the validity of the K–H theory in the boundary layer. The energy dissipation rate in the boundary layer can be estimated as $\varepsilon_{bl} = u_*^3/\lambda_u$, where we use the shear velocity $u_* = \sqrt{\tau_w/\rho} = \sqrt{T/(2\pi\rho r_i^2 L)}$ and the boundary layer thickness $\lambda_u = d/(2Nu_\omega) \sim Re\, G^{-1}$ in a TC turbulent flow (Eckhardt, Grossmann & Lohse 2007). Using the effective scaling $G \sim Re^{1.58}$ obtained in the current system, the energy dissipation rate is found to scale as $\varepsilon_{bl}/(\nu^3 d^{-4}) \sim Re^{2.95}$. Inserting ε_{bl} into the K–H prediction, one obtains $\langle D\rangle/d \sim Re^{-1.2}$, in agreement with the experimental data as well. The scaling exponent -1.2 suggests that the energy dissipation at the boundary layer (ε_{bl}) is just proportional to the local energy dissipation in the bulk of the system (ε_b), which is similar to what is observed for the case of the liquid–liquid dispersion in an agitated vessel (Wichterle 1995). As shown in figure 4(*b*) (green diamonds, approach 2), Weber numbers calculated using ε_{bl} are about 0.08, which is an order of magnitude smaller than the critical value ($O(1)$). This indicates that the energy dissipation rate ε_{bl} near the wall is not large enough to cause the breakup of such small droplets. See Appendix C for more detailed calculations in this part. These results show that the K–H theory is not appropriate for modelling the droplet size in the present system.

A prediction of the droplet size in the non-homogeneous turbulent flow past a solid wall was proposed by Levich (1962), who gave the dynamic pressure force exerted on the two sides of the droplet using the logarithmic distribution of the mean velocity in the boundary layer. Note that the Reynolds number in the current study is in the interval where the logarithmic mean velocity distribution in the boundary layer can exist (Huisman *et al.* 2013). According to Levich (1962), the droplet diameter can be written as $\langle D\rangle = 2\sqrt{\gamma\nu_w/(25\rho_w u_*^3)}$, thus the scaling dependence of the droplet diameter on the Reynolds number is derived as $\langle D\rangle/d \sim Re^{-1.19}$, where the exponent -1.19 is very close to the $-6/5$ in the K–H prediction and agrees again with the scaling dependence observed in experiments for $\phi_o = 1\,\%$. Based on the Levich theory, we also calculate the Weber number as the ratio of the dynamic pressure force induced by the mean flow to the interfacial tension: $We = 25\rho_w u_*^3 \langle D\rangle^2/(2\nu_w\gamma)$. As shown in figure 4(*b*) (blue diamonds, approach 3), the Weber number for the Levich prediction is about 5, which is consistent

with the critical value for the droplet breakup in a turbulent flow (Risso & Fabre 1998; Lemenand *et al.* 2017). The comparison of the Weber numbers based on the energy dissipation rate and that based on Levich's theory lead to the conclusion that the droplet fragmentation, which determines the droplet size, occurs within the boundary layer and is controlled by the dynamic pressure caused by the gradient of mean flow, in agreement with the mechanism originally proposed by Levich. Note that this conclusion also requires that the boundary layer thickness is larger than the droplets diameter, which is supported by the fact that boundary layer thickness is estimated as at least 5 times the droplet size in this study (see table 1).

The discussion of the two approaches above is based on the droplet size at $\phi_o = 1\,\%$, whereas the droplet size at $\phi_o = 99\,\%$ is found to follow the same $-6/5$ scaling dependence (see black triangles in figure 4*a*), indicating the robustness of the scaling law. Furthermore, this figure also shows the existence of the asymmetry of the droplet size between O/W and W/O at high *Re*, at least for low dispersed phase volume fractions (i.e. $\phi_o = 1\,\%$ and $99\,\%$). Considering that the droplet size for W/O is about $50\,\%$ larger than that for O/W, only a slight variation of the Weber number is expected at $\phi_o = 99\,\%$ as compared to the case at $\phi_o = 1\,\%$. Therefore, all the qualitative conclusions given above are valid for emulsions at $\phi_o = 99\,\%$ as well. In this case, the droplet coalescence needs to be considered. The fact that the breakup theory, without accounting for coalescence, describes well the experimental result is particularly interesting. Indeed, for a steady state to be reached finally, the coalescence rate of droplets has to be equal to the breakup rate of coalesced droplets. We therefore observed an average size that is larger than that predicted by the breakup theory, but which remains proportional to it. Note that the interpretation given here is still not complete, and the results remain open for discussion. Additionally, the finding that the droplet formation is controlled by the boundary layer also provides a reasonable explanation for the observations that the droplet size hardly depends on the dispersed phase volume fraction ϕ_d (see figure 4*a*). The droplets that are generated close to the wall, where similar mean velocity gradient could distribute for various ϕ_d, are expected to have similar size. Therefore, the similar droplet size is observed at various ϕ_d in the entire system for O/W (or W/O) emulsions.

Next, we turn to the results using surfactant. Experiments using $250\ \mu\mathrm{l\,l^{-1}}$ DBE are performed, and the results are shown in figure 4(*a*). We note that the scaling dependence of the droplet size on the Reynolds number remains, suggesting the robustness of the scaling law for turbulent emulsions containing DBE. For the case $\phi_o = 1\,\%$, it is found that the droplet size decreases only slightly due to DBE. However, the droplet size at $\phi_o = 99\,\%$ shows a dramatic reduction to a value close to that at $\phi_o = 1\,\%$, yielding the elimination of the asymmetry of the droplet size, for various Reynolds numbers. Since we have found that the recovery of the symmetry using DBE is due to the inhibition of droplet coalescence for the lowest *Re* case (i.e. $Re = 5.2 \times 10^3$), it is reasonable to conclude that the similar behaviours of the droplet size observed here at high *Re* have the same physical interpretations. Moreover, similar results have been observed in additional experiments using a lower concentration of DBE ($12.5\ \mu\mathrm{l\,l^{-1}}$) (see Appendix D).

4. Conclusions

In summary, we investigated the hydrodynamic behaviours of emulsions in a turbulent shear flow by varying the oil volume fraction from $0\,\%$ to $100\,\%$. First, it is found that the average droplet diameter hardly changes with the oil volume fraction for O/W (or W/O) emulsions, while the ethanol–water droplets in W/O are $50\,\%$ larger than the oil

droplets in O/W. Second, the increasing trend of the effective viscosity versus the dispersed phase volume fraction is similar for both O/W and W/O emulsions, whereas the effective viscosity of O/W is found to be higher than that of W/O for the same Reynolds number, particularly for the case of high dispersed phase volume fractions. The asymmetric behaviours of the droplet size and the effective viscosity between O/W and W/O emulsions can be traced back to the presence of unavoidable surface-active contaminants, mainly from the wall, which probably preferentially dissolve in ethanol–water. In the presence of the contaminants, the coalescence of the oil droplets in O/W is suppressed when compared to the ethanol–water droplets with cleaner surface in W/O, yielding the smaller droplet size for O/W than that for its W/O counterpart. Moreover, the higher effective viscosity of O/W than that of W/O can be connected to the smaller and non-deformable oil droplets due to the contaminants. By introducing the oil-soluble surfactant DBE at a controlled concentration, we recover the symmetries of both the droplet size and the effective viscosity between O/W and W/O emulsions. This is consistent with the explanation of the mechanism responsible for the initial asymmetry.

Next, we discuss what sets the droplets size in turbulent emulsions. First, the normalized droplet size is found to be close to a $-6/5$ scaling dependence on the Reynolds number for the oil volume fractions 1 % and 99 %, which is robust for both emulsions with and without surfactant. Theoretically, the $-6/5$ scaling dependence can be obtained using either the K–H theory with the energy dissipation rate or the theory by Levich. However, the Weber numbers being much less than 1 for the K–H theory indicates that the energy dissipation rate in both the bulk flow and the boundary layer is not enough to cause the breakup of such small droplets in this study. According to the Weber number based on Levich's theory, we conclude that the droplet fragmentation, which determines the droplet size, occurs within the boundary layer and is controlled by the dynamic pressure caused by the gradient of mean flow.

The present findings provide a better understanding of the hydrodynamic behaviours for both O/W emulsions and their W/O counterparts. The results on the effective viscosity open the possibility for active drag reduction during the oil recovery and transport through controlling the dispersed phase. Our finding of Levich's droplet fragmentation mechanism also has some potential implications for the modulation of droplet size in chemical processing related to the dynamic emulsification. In future work, more effects that may affect the effective viscosity and droplet size will be studied, aiming at attaining a complete understanding of the hydrodynamic behaviours of the turbulent emulsion at various conditions, and in particular near the phase inversion, where the phenomena are most striking.

Acknowledgements. We acknowledge M. Li, S. Lyu and S. van Aartsen for their insightful suggestions and discussions. We thank O. Masbernat for his help in selecting the surfactants.

Funding. This work is supported financially by the National Natural Science Foundation of China under grant nos 11988102, 91852202, and the Tencent Foundation through the Xplorer Prize.

Declaration of interests. The authors report no conflict of interest.

Author ORCIDs.
Lei Yi https://orcid.org/0000-0002-0247-4600;
Cheng Wang https://orcid.org/0000-0002-6470-7289;
Detlef Lohse https://orcid.org/0000-0003-4138-2255;
Frédéric Risso https://orcid.org/0000-0002-8380-4957;
Federico Toschi https://orcid.org/0000-0001-5935-2332;
Chao Sun https://orcid.org/0000-0002-0930-6343.

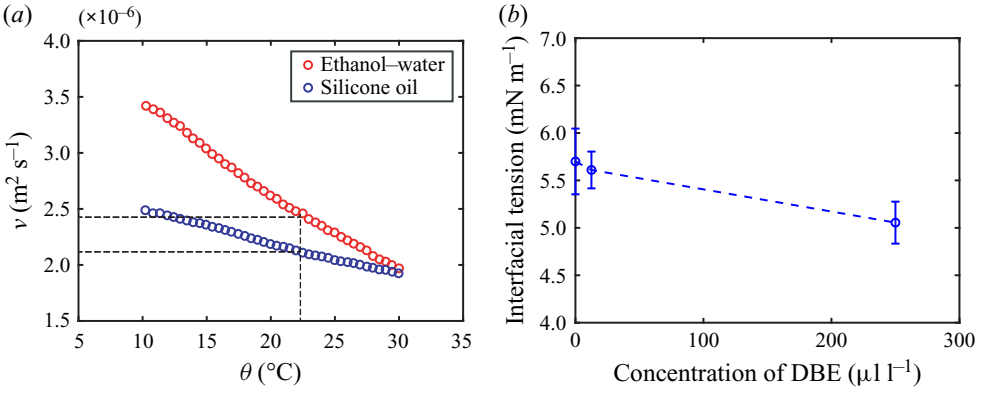

Figure 5. (*a*) The kinematic viscosity ν as a function of the temperature θ. The red circles denote measured viscosity of ethanol–water, and the blue circles depict that of silicone oil. At the temperature for experiments $\theta = 22\,^{\circ}\mathrm{C}$, the viscosity of ethanol–water is $\nu_w = 2.4 \times 10^{-6}$ m^2 s^{-1}, while that of silicone oil is $\nu_o = 2.1 \times 10^{-6}$ m^2 s^{-1}. (*b*) The interfacial tension as a function of the concentration of DBE in oil.

Appendix A. Liquids and surfactants

The silicone oil (KF-96L-2cSt), purchased from Shin-Etsu, has viscosity $\nu_o = 2.1 \times 10^{-6}$ m^2 s^{-1} and density $\rho_o = 866$ kg m^{-3}. The ethanol–water mixture is prepared with 25 % water and 75 % ethanol in volume, and has viscosity $\nu_w = 2.4 \times 10^{-6}$ m^2 s^{-1} and density $\rho_w = 860$ kg m^{-3}, which agree with the literature values (Pires *et al.* 2007; Khattab *et al.* 2012). The water used in the ethanol–water mixture is ultra-pure water, from a water purification system (Milli-Q, Merck, Germany), with electrical conductivity 18.2 MΩ. Note that the viscosity of this mixture is very close to that of silicone oil. The viscosity values of both these two liquid phases are measured using a hybrid rheometer type of TA DHR-1 at temperature $\theta = 22\,^{\circ}\mathrm{C}$ (see figure 5*a*). Apart from the small gap between the shift of the inner cylinder and the upper plate, the TC system is almost closed, which reduces the evaporation of the ethanol. The volume variation of the emulsion before and after the experiments is negligible. The ethanol concentration in the ethanol–water mixture is thus almost constant throughout the measurements.

The density match of these two liquid phases eliminates the effect of centrifugal force on the liquid distribution. Furthermore, the dispersed droplets are expected to experience pressure fluctuations due to the strong turbulent liquid velocity fluctuations that develop in the current system. Here, we can compare the force induced by the velocity fluctuations to the centrifugal force by introducing a centrifugal Froude number (van Gils *et al.* 2013)

$$Fr_{cent}(r) = \frac{\rho u_\theta'^2/\langle D\rangle}{\Delta\rho\, U_\theta^2/r}, \tag{A1}$$

where u_θ' denotes the standard deviation of the azimuthal liquid velocity fluctuations in the bulk, U_θ is the mean azimuthal liquid velocity, and r is the radial position of the droplet to be considered. Based on the measurements in previous studies (Grossmann *et al.* 2016), we take the estimations $u_\theta' \sim 0.01\omega r_i$ and $U_\theta \sim 0.1\omega r_i$. Consequently, we find that $Fr_{cent}(r)$ is of the order of 10^2, indicating that the centrifugal force is negligible compared to the force induced by the velocity fluctuations, which leads the droplets to get uniformly spread in the entire system.

A non-ionic surfactant is used in experiments, which is a kind of dimethylsiloxane block copolymer (30–35 % ethylene oxide) purchased from Gelest. For convenience, we use its abbreviation (DBE) from the manufacturer. The density and molecular weight reported by the manufacturer are 970 kg m^{-3} and around 10^3 g mol^{-1}, respectively. This surfactant is non-soluble in water but highly soluble in silicone oil. The interfacial tension between the two liquids (oil and ethanol–water) was measured using the pendant drop technique on a goniometer instrument (SCA20). Without using surfactant, the interfacial tension between oil and ethanol–water is $\gamma = 5.7$ mN m^{-1}. We performed measurements for emulsions containing DBE at various concentrations. As shown in figure 5(*b*), the interfacial tension between the two liquids decreases only slightly with the increasing concentration of DBE. Considering that the Levich prediction ($\langle D\rangle = 2\sqrt{\gamma\nu/(25\rho u_*^3)}$) gives a scaling between the droplet size and the interfacial tension as $\langle D\rangle \sim \gamma^{1/2}$, we can estimate that the droplet size reduction due to the interfacial tension reduction is around only 5 %, which is much less than the 50 % jump of droplet size measured in experiments with adding 250 µl l^{-1} DBE. The effect of the interfacial tension reduction due to the DBE on the droplet size is unimportant in the current work. Thus it is reasonable to conclude that the inhibition of the droplet coalescence is the dominating factor in affecting the droplet size when using DBE in emulsions.

Appendix B. The torque and the effective viscosity

The torque is a response parameter of the emulsion system in the current study. The torque is measured directly by the rheometer through the shaft connected to the inner rotating cylinder with high accuracy up to 0.1 nN m. For each experiment, we set the angular velocity ω_i of the inner cylinder at a constant value. After the system reaches a statistically stable state, the measurement of the torque is performed.

Note that the total torque (T_{raw}) measured directly by the torque sensor can be split into two parts: (1) the torque T due to the sidewall of the inner cylinder (TC flow); (2) the torque T_{end} related to the top and bottom end plates (von Kármán flow). In this study, what we need is T, which can be determined by using a linearization method (Greidanus *et al.* 2011; Hu *et al.* 2017). We performed torque measurements in three TC devices with different heights, L, $2L$ and $3L$. Since the contribution of the cylindrical sidewall increases linearly with the height of the cylinder (Greidanus *et al.* 2011; Hu *et al.* 2017), we can obtain T_{end} as the longitudinal intercept of the linear fit (see figure 6*a*). The ratio of the torque caused by the TC flow to the total torque can be given as $\beta = 1 - T_{end}/T_{raw}$, which is determined by performing experiments for two cases of single-phase flow (i.e. $\phi_o = 0\,\%$ and 100 %). Then the β obtained can be applied to the flow with internal dispersed phase (i.e. emulsions). Consequently, the value of the torque caused by the TC emulsion flow can be calculated for various oil volume fractions.

For a TC turbulent emulsion, the control parameter can be defined using the modified Reynolds number

$$Re_m = \omega_i r_i d/\nu_{eff}, \tag{B1}$$

where ν_{eff} is the effective viscosity of the emulsion. The response parameter is the modified dimensionless torque given by

$$G_m = T/2\pi L\rho\nu_{eff}^2, \tag{B2}$$

where T denotes the torque that is required to maintain the inner cylinder rotating at a constant angular velocity ω_i.

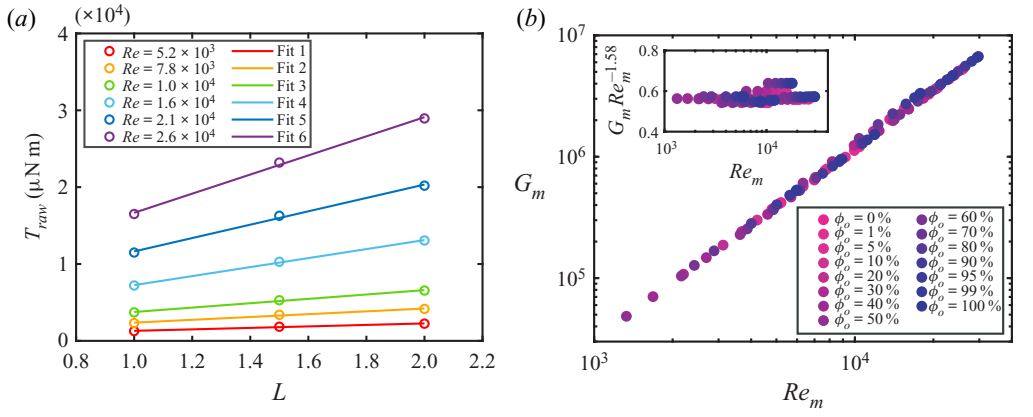

Figure 6. (*a*) The calibration of the torque measurements. The torque contribution of the end effect can be determined as the longitudinal intercept of the fitting line. Here, the oil volume fraction is $\phi_o = 0\,\%$. (*b*) The dependence between the modified dimensionless torque G_m and the modified Reynolds number Re_m, using the effective viscosity. All these sets of data at the various oil volume fractions collapse in a master curve, and the error is less than 1 %. The inset shows the dimensionless torque compensated with $Re_m^{-1.58}$. Here, the results are from emulsions without using surfactant.

First, we calculate the Re_m and G_m at various angular velocities ω_i for pure ethanol–water mixture ($\phi_o = 0\,\%$) with a known viscosity. When we plot these data in a G_m–Re_m plot, we find a scaling law $G_m \sim Re_m^{1.58}$ (see figure 6*b*). Further, we can write this relation as $G_m = K\,Re_m^{1.58}$, where K denotes a constant prefactor. If we insert the definitions of G_m and Re_m into this dependence, we obtain a dependence of torque T and viscosity ν_{eff} as

$$T = AK\nu_{eff}^{0.42}, \tag{B3}$$

where $A = 2\pi L\rho(\omega_i r_i d)^{1.58}$. This relation is expected to be valid for emulsion systems with various oil volume fractions and Reynolds numbers as well, which is supported by previous studies (Ravelet, Delfos & Westerweel 2007; Bakhuis *et al.* 2021). The torque and the effective viscosity of the emulsion system can be denoted as T and ν_{eff} for a constant angular velocity ω_i at the oil volume fraction ϕ_o. For the pure ethanol–water mixture ($\phi_o = 0\,\%$) system at the same angular velocity, we obtain the measured torque value T_w and the viscosity ν_w. Both of these systems follow the relation given above. Since the angular velocities of these two systems are the same, the prefactor A is the same too. Then we can derive the relation

$$\frac{\nu_{eff}}{\nu_w} = \left(\frac{T}{T_w}\right)^{2.38}. \tag{B4}$$

The effective viscosity of emulsion systems ν_{eff} can be obtained based on this relation. By using the effective viscosity obtained for each case, we calculate G_m and Re_m for various volume fractions and angular velocities. When we plot together all data in a G_m–Re_m plot, we find that all data sets of G_m versus Re_m collapse in a master curve, for various oil fractions (see figure 6*b*).

Appendix C. The mechanism on the droplet breakup

In a TC turbulent flow, the boundary layer thickness can be estimated as

$$\lambda_u = d/(2\,Nu_\omega). \tag{C1}$$

Here, we use another typical response parameter in a TC turbulent flow, the angular velocity Nusselt number

$$Nu_\omega = \frac{T}{2\pi L\rho J_\omega^{lam}}, \tag{C2}$$

where $J_\omega^{lam} = 2\nu r_i^2 r_o^2 \omega_i/(r_o^2 - r_i^2)$ is the angular velocity transport for the laminar TC flow.

The droplet size is expected to be dominated by the boundary layer region close to the wall, where the energy dissipation rate (ε_{bl}) is largest (Ezeta *et al.* 2018). The rate ε_{bl} can be estimated as $\varepsilon_{bl} = u_*^3/\lambda_u$, where we use the shear velocity $u_* = \sqrt{\tau_w/\rho} = \sqrt{T/(2\pi\rho r_i^2 L)}$ and the boundary layer thickness $\lambda_u = d/(2Nu_\omega)$ in a TC turbulent flow (Eckhardt *et al.* 2007).

First, we consider the effect of the viscous deformation stress on the breakup, which can be characterized by the capillary number

$$Ca = \tau_v/\tau_r = \frac{\mu\varepsilon^{1/2}\langle D\rangle}{\gamma\nu^{1/2}}, \tag{C3}$$

where $\tau_v = \mu(\varepsilon/\nu)^{1/2}$ is the viscous deforming stress, and $\tau_r = \gamma/\langle D\rangle$ is the restoring stress (interfacial tension). As the energy dissipation rate in the boundary layer is inserted into the above equation ($\varepsilon = \varepsilon_{bl}$), we get $Ca \leqslant 0.04$ (see table 1). In addition, the Kolmogorov length scale in the turbulent boundary layer ($\eta_{bl} = (\nu_w^3/\varepsilon_{bl})^{1/4}$) is found to be smaller than the droplet size. These results suggest that the viscous deformation stress is not important in determining the droplet breakup.

Next, we consider the K–H theory based on the energy dissipation rate in the boundary layer. The normalized energy dissipation rate can be estimated as $\varepsilon_{bl}/(\nu^3 d^{-4}) \sim G^{3/2}\,Nu_\omega$. Since the volume fraction of the dispersed phase is very low here ($\phi_o = 1\,\%$ or $99\,\%$), the viscosity of the emulsion is approximately equal to that of the continuous phase, giving $Re_m \approx Re$ and $G_m \approx G$. Using the effective scaling $G = T/2\pi L\rho\nu^2 \sim Re^{1.58}$ obtained in the current system (see figure 6*b*), we can get $Nu_\omega \sim Re^{0.58}$. Consequently, the energy dissipation rate is found to scale as $\varepsilon_{bl}/(\nu^3 d^{-4}) \sim Re^{2.95}$. Inserting this expression for ε_{bl} into the K–H prediction (i.e. $\langle D\rangle = C(\rho/\gamma)^{-3/5}\varepsilon_{bl}^{-2/5}$), one obtains $\langle D\rangle/d \sim Re^{-1.18}$, which is also in good agreement with the experimental data. However, the Weber numbers calculated using ε_{bl} are about 0.08, which is an order of magnitude smaller than the critical value ($O(1)$), suggesting that the K–H theory is not appropriate for modelling the droplet size in the present system.

The viscous sublayer thickness is estimated as $\delta_{vis} = 5\nu/u_*$. The droplet size is found to be comparable with the viscous sublayer thickness (see $\langle D\rangle/\delta_{vis}$ in table 2). We found that even in the viscous sublayer where the shear rate is higher, the Ca values (around 0.1–0.2) are still much smaller than 1. This supports that the droplet breakup is dominated by the inertial force, instead of the viscous shear stress. Additionally, the exclusion of the droplets from the viscous sublayer could also be a reason for the reduced effectiveness of larger drops on the effective viscosity for the W/O emulsions (see figure 2*b*).

Re	5.2×10^3	7.8×10^3	1.0×10^4	1.6×10^4	2.1×10^4	2.6×10^4
$\langle D \rangle / \delta_{vis}$ (O/W)	0.8	0.7	0.6	0.6	0.5	0.5
$\langle D \rangle / \delta_{vis}$ (W/O)	1.4	1.3	1.1	1.0	0.8	0.8

Table 2. The ratios of the droplet size to the viscous sublayer thickness for the O/W ($\phi_o = 1\,\%$) and W/O ($\phi_o = 99\,\%$) cases.

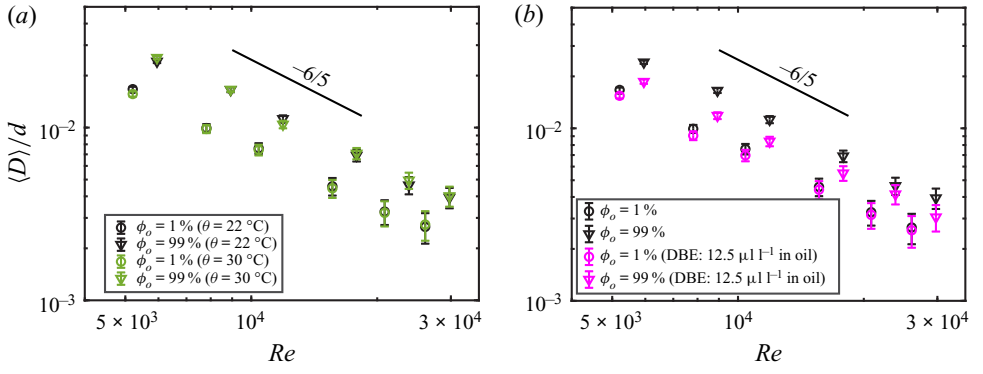

Figure 7. (*a*) The droplet size for various Reynolds numbers at $\theta = 22\,^{\circ}$C and at $\theta = 30\,^{\circ}$C. (*b*) The average droplet diameter normalized by the gap width as a function of the Reynolds number for oil volume fractions $\phi_o = 1\,\%$ and $99\,\%$. The black and magenta symbols denote droplet sizes in emulsions using no surfactant and using 12.5 µl l^{-1} DBE, respectively. The black lines denote the scaling prediction of the K–H theory. The asymmetry of the droplet size in O/W ($\phi_o = 1\,\%$) and W/O ($\phi_o = 99\,\%$) emulsions is partially removed using 12.5 µl l^{-1} DBE.

Appendix D. Additional experiments

One may think that the difference between the viscosities of oil ($\nu_o = 2.1 \times 10^{-6}$ m^2 s^{-1}) and ethanol–water ($\nu_w = 2.4 \times 10^{-6}$ m^2 s^{-1}) could be the source of the asymmetry of the droplet size. By adjusting the temperature of the emulsion from $\theta = 22\,^{\circ}$C to $\theta = 30\,^{\circ}$C, we eliminate the viscosity difference between the two liquids (see figure 5*a*) and measure the droplet size at oil volume fractions $\phi_o = 1\,\%$ and $99\,\%$. As shown in figure 7(*a*), the droplet sizes have only a slight change when compared to the results obtained at $\theta = 22\,^{\circ}$C. Clearly, the ethanol–water droplets in W/O are larger than the oil droplets in O/W as well, for all Reynolds numbers. Thus this small viscosity difference between the two liquids used in experiments cannot account for the obvious asymmetry of the droplet size.

Here, we provide experimental results for emulsions using 12.5 µl l^{-1} DBE. As shown in figure 7(*b*), the $-6/5$ scaling dependence of the droplet size on the Reynolds number remains, suggesting the robustness of the scaling law for turbulent emulsions containing 12.5 µl l^{-1} DBE. For the case $\phi_o = 1\,\%$, it is found that the droplet size decreases only slightly due to DBE. However, the droplet size at $\phi_o = 99\,\%$ shows an obvious reduction, yielding the partial elimination of the asymmetry of droplet size, for various Reynolds numbers.

References

Afshar Ghotli, R., Raman, A.A.A., Ibrahim, S. & Baroutian, S. 2013 Liquid–liquid mixing in stirred vessels: a review. *Chem. Eng. Commun.* **200** (5), 595–627.

Bakhuis, D., Ezeta, R., Bullee, P.A., Marin, A., Lohse, D., Sun, C. & Huisman, S.G. 2021 Catastrophic phase inversion in high-Reynolds-number turbulent Taylor–Couette flow. *Phys. Rev. Lett.* **126** (6), 064501.

Bakhuis, D., Verschoof, R.A., Mathai, V., Huisman, S.G., Lohse, D. & Sun, C. 2018 Finite-sized rigid spheres in turbulent Taylor–Couette flow: effect on the overall drag. *J. Fluid Mech.* **850**, 246–261.

Baret, J.-C. 2012 Surfactants in droplet-based microfluidics. *Lab on a Chip* **12** (3), 422–433.

Batchelor, G.K. 1953 *The Theory of Homogeneous Turbulence*. Cambridge University Press.

Bazazi, P. & Hejazi, S.H. 2020 Retarding spreading of surfactant drops on solid surfaces: interplay between the Marangoni effect and capillary flows. *Phys. Rev. Fluids* **5** (8), 084006.

Boxall, J.A., Koh, C.A., Sloan, E.D., Sum, A.K. & Wu, D.T. 2012 Droplet size scaling of water-in-oil emulsions under turbulent flow. *Langmuir* **28** (1), 104–110.

Calvo, E., de Malmazet, E., Risso, F. & Masbernat, O. 2019 Coalescence of water drops at an oil–water interface loaded with microparticles and surfactants. *Ind. Engng Chem. Res.* **58** (34), 15573–15587.

Cristini, V., Bławzdziewicz, J. & Loewenberg, M. 1998 Near-contact motion of surfactant-covered spherical drops. *J. Fluid Mech.* **366**, 259–287.

Dai, B. & Leal, L.G. 2008 The mechanism of surfactant effects on drop coalescence. *Phys. Fluids* **20** (4), 040802.

De Malmazet, E., Risso, F., Masbernat, O. & Pauchard, V. 2015 Coalescence of contaminated water drops at an oil/water interface: influence of micro-particles. *Colloids Surf.* (A) **482**, 514–528.

De Vita, F., Rosti, M.E., Caserta, S. & Brandt, L. 2019 On the effect of coalescence on the rheology of emulsions. *J. Fluid Mech.* **880**, 969–991.

Duineveld, P.C. 1995 The rise velocity and shape of bubbles in pure water at high Reynolds number. *J. Fluid Mech.* **292**, 325–332.

Eckhardt, B., Grossmann, S. & Lohse, D. 2007 Torque scaling in turbulent Taylor–Couette flow between independently rotating cylinders. *J. Fluid Mech.* **581**, 221–250.

Erni, P. 2011 Deformation modes of complex fluid interfaces. *Soft Matt.* **7** (17), 7586–7600.

Eskin, D., Taylor, S.D. & Yang, D. 2017 Modeling of droplet dispersion in a turbulent Taylor–Couette flow. *Chem. Engng Sci.* **161**, 36–47.

Ezeta, R., Huisman, S.G., Sun, C. & Lohse, D. 2018 Turbulence strength in ultimate Taylor–Couette turbulence. *J. Fluid Mech.* **836**, 397–412.

de Gennes, P.-G. 2001 Some remarks on coalescence in emulsions or foams. *Chem. Engng Sci.* **56** (19), 5449–5450.

van Gils, D.P.M., Guzman, D.N., Sun, C. & Lohse, D. 2013 The importance of bubble deformability for strong drag reduction in bubbly turbulent Taylor–Couette flow. *J. Fluid Mech.* **722**, 317–347.

van Gils, D.P.M., Bruggert, G.-W., Lathrop, D.P., Sun, C. & Lohse, D. 2011 The Twente turbulent Taylor–Couette (T3C) facility: strongly turbulent (multiphase) flow between two independently rotating cylinders. *Rev. Sci. Instrum.* **82** (2), 025105.

Greidanus, A.J., Delfos, R. & Westerweel, J. 2011 Drag reduction by surface treatment in turbulent Taylor–Couette flow. *J. Phys.: Conf. Ser.* **318** (8), 082016.

Grossmann, S., Lohse, D. & Sun, C. 2016 High-Reynolds number Taylor–Couette turbulence. *Annu. Rev. Fluid Mech.* **48**, 53–80.

Guazzelli, É. & Pouliquen, O. 2018 Rheology of dense granular suspensions. *J. Fluid Mech.* **852**, P1.

Ha, J.W., Yoon, Y. & Leal, L.G. 2003 The effect of compatibilizer on the coalescence of two drops in flow. *Phys. Fluids* **15** (4), 849–867.

Hesketh, R.P., Etchells, A.W. & Russell, T.W.F. 1991*a* Bubble breakage in pipeline flow. *Chem. Engng Sci.* **46** (1), 1–9.

Hesketh, R.P., Etchells, A.W. & Russell, T.W.F. 1991*b* Experimental observations of bubble breakage in turbulent flow. *Ind. Engng Chem. Res.* **30** (5), 835–841.

Hinze, J.O. 1955 Fundamentals of the hydrodynamic mechanism of splitting in dispersion processes. *AIChE J.* **1** (3), 289–295.

Hu, H., Wen, J., Bao, L., Jia, L., Song, D., Song, B., Pan, G., Scaraggi, M., Dini, D., Xue, Q., *et al.* 2017 Significant and stable drag reduction with air rings confined by alternated superhydrophobic and hydrophilic strips. *Sci. Adv.* **3** (9), e1603288.

Huisman, S.G., Scharnowski, S., Cierpka, C., Kähler, C.J., Lohse, D. & Sun, C. 2013 Logarithmic boundary layers in strong Taylor–Couette turbulence. *Phys. Rev. Lett.* **110** (26), 264501.

KATO, S., NAKAYAMA, E. & KAWASAKI, J. 1991 Types of dispersion in agitated liquid–liquid systems. *Can. J. Chem. Engng* **69** (1), 222–227.

KAWAGUCHI, M. 2016 Silicone oil emulsions stabilized by polymers and solid particles. *Adv. Colloid Interface Sci.* **233**, 186–199.

KHATTAB, I.S., BANDARKAR, F., FAKHREE, M.A.A. & JOUYBAN, A. 2012 Density, viscosity, and surface tension of water + ethanol mixtures from 293 to 323 K. *Korean J. Chem. Engng* **29** (6), 812–817.

KOLMOGOROV, A. 1949 On the breakage of drops in a turbulent flow. *Dokl. Akad. Nauk. SSSR* **66**, 825–828.

KUMAR, S. 1996 On phase inversion characteristics of stirred dispersions. *Chem. Engng Sci.* **51** (5), 831–834.

LALANNE, B., MASBERNAT, O. & RISSO, F. 2020 Determination of interfacial concentration of a contaminated droplet from shape oscillation damping. *Phys. Rev. Lett.* **124** (19), 194501.

LEMENAND, T., DELLA VALLE, D., DUPONT, P. & PEERHOSSAINI, H. 2017 Turbulent spectrum model for drop-breakup mechanisms in an inhomogeneous turbulent flow. *Chem. Engng Sci.* **158**, 41–49.

LEMENAND, T., DELLA VALLE, D., ZELLOUF, Y. & PEERHOSSAINI, H. 2003 Droplets formation in turbulent mixing of two immiscible fluids in a new type of static mixer. *Intl J. Multiphase Flow* **29** (5), 813–840.

LEVICH, V.G. 1962 *Physicochemical Hydrodynamics*. Prentice-Hall Inc.

MAFFI, J.M., MEIRA, G.R. & ESTENOZ, D.A. 2021 Mechanisms and conditions that affect phase inversion processes: a review. *Can. J. Chem. Engng* **99** (1), 178–208.

MANDAL, A., SAMANTA, A., BERA, A. & OJHA, K. 2010 Characterization of oil–water emulsion and its use in enhanced oil recovery. *Ind. Engng Chem. Res.* **49** (24), 12756–12761.

MANIKANTAN, H. & SQUIRES, T.M. 2020 Surfactant dynamics: hidden variables controlling fluid flows. *J. Fluid Mech.* **892**, P1.

MCCLEMENTS, D.J. 2007 Critical review of techniques and methodologies for characterization of emulsion stability. *Crit. Rev. Food Sci. Nutr.* **47** (7), 611–649.

PACEK, A.W., NIENOW, A.W. & MOORE, I.P.T. 1994 On the structure of turbulent liquid–liquid dispersed flows in an agitated vessel. *Chem. Engng Sci.* **49** (20), 3485–3498.

PAL, R. 1996 Effect of droplet size on the rheology of emulsions. *AIChE J.* **42** (11), 3181–3190.

PERAZZO, A., PREZIOSI, V. & GUIDO, S. 2015 Phase inversion emulsification: current understanding and applications. *Adv. Colloid Interface Sci.* **222**, 581–599.

PERLEKAR, P., BIFERALE, L., SBRAGAGLIA, M., SRIVASTAVA, S. & TOSCHI, F. 2012 Droplet size distribution in homogeneous isotropic turbulence. *Phys. Fluids* **24** (6), 065101.

PIELA, K., OOMS, G. & SENGERS, J.V. 2009 Phenomenological description of phase inversion. *Phys. Rev.* E **79** (2), 021403.

PIRES, R.M., COSTA, H.F., FERREIRA, A.G.M. & FONSECA, I.M.A. 2007 Viscosity and density of water + ethyl acetate + ethanol mixtures at 298.15 and 318.15 K and atmospheric pressure. *J. Chem. Engng Data* **52** (4), 1240–1245.

POUPLIN, A., MASBERNAT, O., DÉCARRE, S. & LINÉ, A. 2011 Wall friction and effective viscosity of a homogeneous dispersed liquid–liquid flow in a horizontal pipe. *AICHE J.* **57** (5), 1119–1131.

RAVELET, F., DELFOS, R. & WESTERWEEL, J. 2007 Experimental studies of liquid–liquid dispersion in a turbulent shear flow. In *Advances in Turbulence XI* (ed. J.M.L.M. Palma & A. Silva Lopes), pp. 331–333. Springer.

RHEINGANS, O., HUGENBERG, N., HARRIS, J.R., FISCHER, K. & MASKOS, M. 2000 Nanoparticles built of cross-linked heterotelechelic, amphiphilic poly (dimethylsiloxane)-b-poly (ethylene oxide) diblock copolymers. *Macromolecules* **33** (13), 4780–4790.

RISSO, F. & FABRE, J. 1998 Oscillations and breakup of a bubble immersed in a turbulent field. *J. Fluid Mech.* **372**, 323–355.

ROSTI, M.E., GE, Z., JAIN, S.S., DODD, M.S. & BRANDT, L. 2019 Droplets in homogeneous shear turbulence. *J. Fluid Mech.* **876**, 962–984.

ROSTI, M.E. & TAKAGI, S. 2021 Shear-thinning and shear-thickening emulsions in shear flows. *Phys. Fluids* **33** (8), 083319.

SALAGER, J.-L., MÁRQUEZ, L., PEÑA, A.A., RONDÓN, M., SILVA, F. & TYRODE, E. 2000 Current phenomenological know-how and modeling of emulsion inversion. *Ind. Engng Chem. Res.* **39** (8), 2665–2676.

SOLIGO, G., ROCCON, A. & SOLDATI, A. 2020 Effect of surfactant-laden droplets on turbulent flow topology. *Phys. Rev. Fluids* **5** (7), 073606.

STICKEL, J.J. & POWELL, R.L. 2005 Fluid mechanics and rheology of dense suspensions. *Annu. Rev. Fluid Mech.* **37**, 129–149.

SUNDARARAJ, U. & MACOSKO, C.W. 1995 Drop breakup and coalescence in polymer blends: the effects of concentration and compatibilization. *Macromolecules* **28** (8), 2647–2657.

TOBIN, T. & RAMKRISHNA, D. 1999 Modeling the effect of drop charge on coalescence in turbulent liquid–liquid dispersions. *Can. J. Chem. Engng* **77** (6), 1090–1104.

VAN GILS, D.P.M., HUISMAN, S.G., GROSSMANN, S., SUN, C. & LOHSE, D. 2012 Optimal Taylor–Couette turbulence. *J. Fluid Mech.* **706**, 118–149.

VERSCHOOF, R.A., VAN DER VEEN, R.C.A., SUN, C. & LOHSE, D. 2016 Bubble drag reduction requires large bubbles. *Phys. Rev. Lett.* **117** (10), 104502.

WICHTERLE, K. 1995 Drop breakup by impellers. *Chem. Engng Sci.* **50** (22), 3581–3586.

YI, L., TOSCHI, F. & SUN, C. 2021 Global and local statistics in turbulent emulsions. *J. Fluid Mech.* **912**, A13.

ZAMBRANO, N., TYRODE, E., MIRA, I., MARQUEZ, L., RODRÍGUEZ, M.-P. & SALAGER, J.-L. 2003 Emulsion catastrophic inversion from abnormal to normal morphology. 1. Effect of the water-to-oil ratio rate of change on the dynamic inversion frontier. *Ind. Engng Chem. Res.* **42** (1), 50–56.